IAC–21–66736

ARGOS: calibrated facility for Image based Relative Navigation technologies on ground verification and testing

Margherita Piccinin,[*] Stefano Silvestrini,[†] Giovanni Zanotti,[‡] Andrea Brandonisio,[§] Paolo Lunghi,[¶] and Michèle Lavagna[**]

This paper presents the recent developments of ARGOS, a GNC experimental facility at Politecnico of Milano, at the premises of the Aerospace Science and Technology Department (DAER). The purpose of the facility is the testing of novel image-based Guidance, Navigation and Control (GNC) algorithms for autonomous navigation in proximity of a known or unknown uncooperative target. The facility calibration is presented, along with the set-up for the a moon landing and debris fly-around scenario, as representatives of the facility possibilities. In the paper the capability of reproducing realistic and high fidelity images in different operating conditions is verified, by means of a validation process based on synthetic ground truth images.

keywords: GNC Facility, Optical Calibration, Dense Point Cloud Reconstruction, Pose estimation, On ground Testing, Images validation

1. Introduction

To be accepted for flight, Guidance Navigation and Control (GNC) algorithms require running Hardware/Processor-In-the-Loop (HIL/PIL) tests campaigns in highly representative environment. To support this phase, Politecnico di Milano developed the Advanced Robotics & GNC Optical-based Simulator (ARGOS), an experimental facility to support such tests for image-based GNC algorithms [5].

PIL and HIL experiments are mandatory to further increase the Technology Readiness Level (TRL) of image-based navigation algorithms. There are several reasons for which such experimental approach is fundamental for the testing and validation process. In first place, vision-based algorithms development widely relies on synthetic images, because of the scarce availability of complete and repeatable real imagery datasets. To validate such approach, experiments are necessary. In addition, while synthetic images allow to create large datasets, they are not always suitable for carrying out closed-loop PIL tests. In fact, the high computational cost of the rendering process may not allow real time tests, which may thus require the use of a real camera. Finally, the whole navigation system performance can be assessed only by means of complete HIL tests, connecting the composing parts together to verify mutual influences.

In addition to traditional image-based navigation techniques, the recent development of AI-based navigation algorithms has posed further challenges to the verification and testing of the GNC chain [9]. In fact, the images used for training and testing the AI technique require to be highly of the representative of the real space target, otherwise potentially mining the robustness of such black-box algorithms.

ARGOS facility offers multiple configurations, covering different space mission scenarios, including both natural and artificial targets. The facility is equipped with a lunar terrain diorama for planetary landing, satellites and asteroids mock-ups for proximity operations reproduction. The tip of 6 DoF robotic arm hosts the navigation sensors; the arm is controlled so that its tip follows the trajectory risen from the desired spacecraft dynamics in proximity of the target. Two sets of LEDs - manually orientable to tune the illumination conditions with respect to target - complete the infrastructure. The goal is to reproduce a proximity navigation over a scaled but realistic environment. The system is designed to verify either hardware and software breadboards up to TRL

[*]PhD Student, Politecnico di Milano, Italy, margherita.piccinin@polimi.it
[†]Postdoctoral Researcher, Politecnico di Milano, Italy, stefano.silvestrini@polimi.it
[‡]PhD Student, Politecnico di Milano, Italy, giovanni.zanotti@polimi.it
[§]PhD Student, Politecnico di Milano, Italy, andrea.brandonisio@polimi.it
[¶]Assistant Professor, Politecnico di Milano, Italy, paolo.lunghi@polimi.it
[**]Full Professor, Politecnico di Milano, Italy, michelle.lavagna@polimi.it

4, with the possibility to update the system in the future to carry out also real-time hardware-in-the-loop simulations to qualify GNC technologies up to TRL 5.

The features offered and scenarios supported by the facility are discussed in the paper, with a deep insight on the activities which led to the current level of precision the hardware infrastructure offers. As representative of ARGOS capabilities, the paper discusses the set-ups for testing image based navigation according to two currently relevant scenarios: a Moon landing and a Space Debris inspecting and flying around. To be properly employed, the facility requires to be calibrated. This paper proposes a vision-based calibration procedure consisting in reconstructing a dense point-cloud of the target for obtaining a ground truth with the needed accuracy, possibly overcoming the issues related with manufacturing errors. Another approach is also considered, i.e. exploiting the ground truth available prior to manufacturing. The accuracy in terms of images appearance obtained with the two approaches is discussed, highlighting benefits and limitations. Finally, an imaging campaign for validating the produced images is conducted, retrieving the ground truth camera pose by means of optical markers. The obtained images are compared to the corresponding synthetic images and employed for the algorithm testing. Results are critically presented, confirming the adequacy to adopt the proposed technique to successfully calibrate the facility with the required level of accuracy for a broad set of applications.

The paper is structured as follows. In Section 2 ARGOS facility is described in detail; then, in Section 3 the consolidated facility calibration procedures are explained. In Section 4 the experimental set-ups for a lunar landing and debris fly-around scenario are described, starting from the scenarios requirements and then presenting the facility images validation approach. The results for the two set-ups are discussed in Section 5 and the conclusions are reported in Section 6.

2. Experimental facility

This section presents the ARGOS (Advanced Robotics & GNC Optical-based Simulator) facility at PoliMi, which comprises the fundamental following elements:

- Robotic arm.
- Navigation camera.
- Illumination system.
- Moon diorama.
- Artificial satellite mock-up.

Robotic arm The foundation of the analogue facility is based on the robotic arm, which is in charge of simulating the spacecraft motion and dynamics for various mission scenarios. The control and modification of any aspect of the arm behaviour is something achievable through the open architecture of both the robot's hardware and softwarem, giving also the possibility to include additional sensor information in the control loop. The operative envelope of the arm is approximately defined by a 1 m radius, allowing to simulate different scaled trajectories of the spacecraft motion. In the case of the landing simulation scenario the motion of the satellite only is reproduced, while for in-orbit relative motion, the arm trajectory represents the superposition of chaser and target motion.

The sensor suite, namely a navigation camera, is carried at the end-effector of the arm.

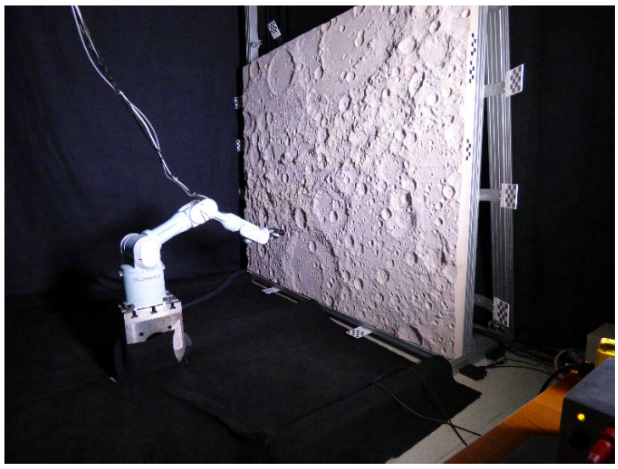

Fig. 1: Optical navigation for landing. Moon diorama and robotic arm in the illumination controlled facility at DAER-Polimi

Navigation camera The main sensor of the reproduced autonomous GNC architecture is made up by the navigation camera, representation of a possible flight hardware. Considering that the focus of the study is the navigation around targets from the final approach phase, a camera with a wide field of view (FoV) and fixed focus is exploited, without the need of having high resolutions. For this facility, a Chameleon 3 by FLIR is used, whose characteristics

Table 1: Navigation camera specifications.

Parameter	Value
Resolution	1280x1024
Frame rate	149
Megapixels	1.3
Chroma	Colour/grey-scale
ADC	10 bit
Sensor format	1/2-inch-type CCD
Focal length	6 mm
FoV	63.5°

are reported in Table 1. Such camera can be easily tuned through a dedicated C++ API, and can be interfaced to the rest of the system by USB3.1 connection and a programmable GPIO. Given that the specifications by datasheet are much better than the requirements imposed, a grey-scale images configuration is adopted for simulating flight hardware, exploiting lower frame rate and a 1024×1024 resolution.

Illumination system In order to properly validate the proposed autonomous GNC algorithms, it is fundamental to ensure a proper illumination and environmental conditions for obtaining realistic images. To achieve that, the light shall not be diffuse, given that the operational conditions under investigation all outside the atmosphere. For such reason, the facility has been realized in a dedicated dark room, preventing light reflection with black curtains and floor covers. To simulate the Sun illumination, a dedicated high-CRI LED array with 60° beam angle and 5700K light temperature is employed, characterised by the features in Table 2.

Table 2: Illumination system specifications

Parameter	Value
Light temperature	5700 K
Beam angle	60°
Led array dimension	1024x1024

Moon diorama A portion of the Far-Side Lunar surface has been realized fully at the PoliMi-Daer laboratories, to be exploited as a mock-up for the landing simulations. To guarantee correct optical properties, the material used for the diorama is Urethane foam due to its surface finish. The diorama is made up by 8 separated tiles, measuring 1200×500 mm, leading to an overall size of 2400×2000 mm and a scale factor of 2000:1. In order to have mixed terrain features, i.e. form plains to rough slopes, a Digital Elevation Model (DEM) from the GLD-100 NASA LROC dataset has been selected. The facility was designed to test navigation algorithms for pinpoint landing with desired touch-down accuracy in the order of 10 m, which in the scaled mock-up corresponds to 5 mm. In order to keep a terrain resolution of at least one order of magnitude better than the required accuracy, the machine-working accuracy of at least 0.5 mm was required. In any case, the 2000:1 can be considered as the maximum scale factor, since, given the fractal structure of the Moon surface, a wide range of altitude can be simulated, from orbit to touchdown.

Artificial satellite mock-up The satellite mock-up is representative of ENVISAT satellite. The ENVISAT mock-up is 1:50 scale of the real one, entailing all the most critical geometrical and appearance features. The mock-up is manufactured using 3D Stratasys Fortus450 3D printer available at Politecnico di Milano premises. The model dimensions are maximized to reduce the scaling of the experiment, compliant with the printer capabilities. In this way, the accuracy to validate the algorithms can be reached. A spray acrylic white paint, usually used for modeling, was applied twice on the surface to reproduce the surface of the spacecraft. The details were adjusted by a thin brush. Silver aluminum foils were used to reproduce the classical thermal protection of spacecraft, made of MultiLayer Insulation (MLI). The white paint and silver aluminum foil have been applied to maximize the reflectivity of the materials and enhance the contrast with respect to the laboratory background.

3. Facility calibration

In this section the facility calibration procedures are presented. In particular, they comprise the camera calibration, the moon diorama calibration via dense reconstruction and the visual markers calibration for pose retrieval.

3.1 *Camera calibration*

A fundamental aspect of vision-based navigation algorithms consists in associating pixel coordinates of image points to real world coordinates. In order to allow this process, the camera model needs to be characterized by means of a calibration, which consists in retrieving the intrinsic camera matrix K and the camera distortion coefficients.

A simple pinhole camera model is characterised by

its intrinsic matrix:

$$K = \begin{bmatrix} f_x & 0 & p_x \\ 0 & f_y & p_y \\ 0 & 0 & 1 \end{bmatrix} \quad [1]$$

where f_x and f_y are the camera focal lengths and (p_x, p_y) is the position of the principal point [3]. The intrinsic camera matrix transforms the coordinates of a point form the camera frame to the image pixel coordinates $\mathbf{x_{px}} = [x_{px}\ y_{px}\ 1]^T$ by means of a projective transformation. To obtain the camera coordinates of the point, a homogeneous transformation is applied to the point homogeneous world coordinates $\mathbf{x_w^H} = [x_w\ y_w\ z_w\ 1]^T$.

$$\mathbf{x_{px}} = K[\mathbf{R_w^c}|\mathbf{t}]\mathbf{x_w^H} \quad [2]$$

where $\mathbf{R_w^c}$ is the rotation matrix from world to camera coordinates and $\mathbf{t}$ the translation vector.

Camera distortion For a real camera model, the two main distortion effects are considered, being the radial and tangential distortion.

Regarding the radial distortion, the actual projected point pixel coordinates (x'', y'') are related to the ideal point coordinates (x', y') by a radial displacement described as:

$$\begin{bmatrix} x'' \\ y'' \end{bmatrix} = L(r') \begin{bmatrix} x' \\ y' \end{bmatrix} \quad [3]$$

where $r' = \sqrt{x'^2 + y'^2}$ is the radial distance from the center and $L(r') = 1 + k_1 r' + k_2 r'^2 + k_3 r'^3 + ...$ is an approximation of an arbitrary function.

Tangential distortion can be corrected applying the following transformation:

$$\begin{aligned} x' &= x'' + [p_1(r''^2 + 2x''^2) + 2p_2 x'' y''] \\ y' &= y'' + [p_2(r''^2 + 2y''^2) + 2p_1 x'' y''] \end{aligned} \quad [4]$$

Calibration procedure A classical chessboard-based calibration procedure is followed in order to retrieve the camera intrinsic parameters, exploiting the OpenCV library [1].

The traditional procedure consists in finding the internal chessboard corners pixel coordinates and associate them to their world coordinates, knowing the chessboard dimensions and lying the corners on the same plane. Several images of the chessboard are taken, from different viewing angles, allowing to estimate the intrinsic matrix and distortion parameters [3]. First, the intrinsic parameters are initially computed, assuming no distortion. Then, the initial camera pose is estimated, solving the Perspective n Point problem (PnP) [2]. Finally, the global Levenberg-Marquardt optimization algorithm is employed to minimize the reprojection error.

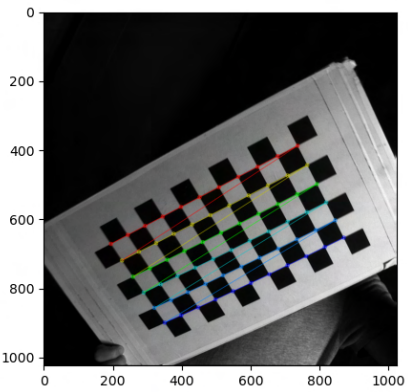

Fig. 2: Camera calibration.

3.2 *Moon diorama dense reconstruction*

The actual target model is generally different from the numerical model, due to imperfections during the production process. Dense matching method has been selected to perform the shape reconstruction: several photos from different angles are taken; then, structure from motion algorithms are used to obtain the camera pose for each image. Finally, dense cloud point models are obtained by triangulation of optical features between different frames. For the Lunar terrain mock-up, reconstruction is performed for the testing region. The dense reconstruction is composed of three main steps:

- Feature detection and extraction.
- Feature matching and geometric verification.
- Structure and motion reconstruction.
- Multi-view stereo and dense reconstruction.

Fig. 3 shows a reconstructed point cloud of a limited testing region, refined through Screened Poisson surface reconstruction.

3.3 *Camera pose estimation in calibrated facility*

The presented work is based on images acquisition without the employment of the robotic arm. In this case, it is possible to derive the camera pose using visual markers applied on the target or in the target proximity.

The marker calibration procedure simply consists in the marker positioning and measurement. The

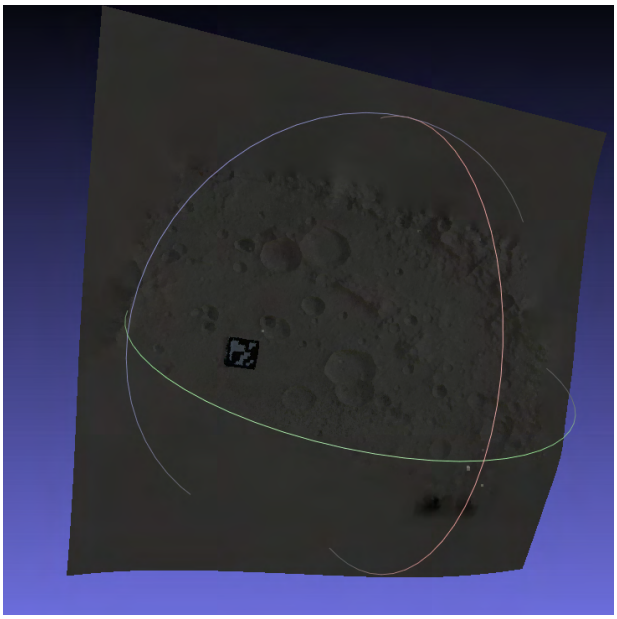

Fig. 3: Dense point cloud reconstruction of testing region.

marker center position is measured with respect to a known point on the target, while its orientation is fixed in order to easily derive a known rotation with respect to the target frame. Thus the camera pose in the world frame is given by:

$$\mathbf{x_{c,w}} = \mathbf{t_{m,w}} + \mathbf{x_{c,m}} \quad [5]$$

$$\mathbf{R_c^w} = \mathbf{R_c^m R_m^w} \quad [6]$$

As shown in Fig. 4, aruco markers are employed, exploiting a predefined dictionary of 50 7-pixels markers.

The camera pose in the marker frame can be derived exploiting a single marker or from multiple markers.

4. Facility set-ups for images acquisition

After the facility calibration, an images acquisition campaign has been conducted for two possible scenarios: a lunar landing and a debris inspection. In this section the facility set-ups adopted for relative navigation technologies testing is described.

4.1 *Moon landing*

The first application for which we needed to collect the image dataset is related to the moon landing. The objective is having an autonomous vision-based navigation system for the lunar landing through artificial

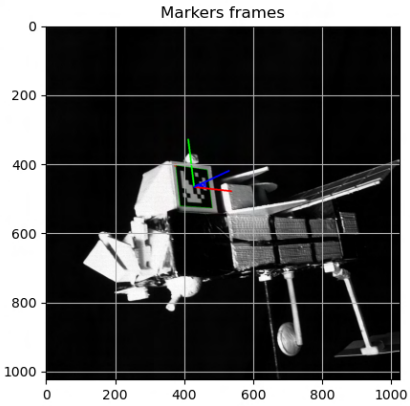

Fig. 4: Visual marker for pose retrieval.

intelligence techniques [8]. The scenario is based on a spacecraft descent trajectory starting from 100km altitude down to 3km altitude targeting the Lunar South Pole. In order to correctly simulate the potential descent trajectory some requirements must be taken into account to set-up the facility to acquire a realistic sequence of camera images. Therefore, the facility must be able to reproduce the conditions listed in Tab. 3.

Table 3: List of the facility requirements for the Moon scenario.

Variable	**Range**
Altitude	3-100 km
Attitude pitch	0°-20°
Sun Elevation angle	0°-90°
Sun Azimuth angle	0°-360°
Craters dimension	0-500m
Craters frequency	1.8e6-3e6

4.2 *Space Debris inspection*

The second scenario studied concerns a relative vision-based navigation system for debris or space object inspection or capture. In particular, the objective was to acquire the image dataset of a trajectory around Envisat to demonstrate the possibility of performing relative navigation with an artificial intelligence feature detection algorithm. The relevant operational scenario where the performance of the vision-based navigation have to be assessed is the short-range operations. In Tab. 4 the facility requirements for the Envisat inspection are listed.

Table 4: List of the facility requirements for the Envisat scenario.

Variable	Range
Chaser relative position	0.5-50 m
Camera attitude pitch/yaw angle	±90°
Sunlight direction azimuth angle	0°-360°
Target attitude angle	0°-360°

4.3 *Accuracy evaluation*

To verify the accuracy of the calibrated facility, images taken with a real camera in a laboratory environment are compared with the synthetic images generated by a rendering software. The validation aim is to verify the reliability of laboratory images by means of quantitative indices, comparing them with synthetic images consistent with the two scenarios. In particular, the synthetic images are generated exploiting the ESA's software Pangu for the moon landing scenario, whereas the open source Blender suite for the debris inspection scenario.

For each scenario, the validation set is made of 10 images spanning the dataset ranges in terms of illumination and poses.

Four indications are examined to evaluate the facility images goodness:

1. **Image histogram**. The histograms information is a low level information which gives a good representation of the image content. Such method has been already used to evaluate images quality for testing of space navigation algorithms [4].

2. **Shadow index**. The synthetic and laboratory images are thresholded to identify shadows. The value of the threshold is identified automatically using the Otsu algorithm. The Otsu method is a deterministic and automatic way to discriminate shadowy and illuminated target parts. Then, the two resulting binary images are subtracted to obtain a shadow disparity map. The accuracy of the shadow representation, which can be considered as representative of the accuracy of the general shape of the sample, is evaluated by a scalar shadow index (J_s), defined as:

$$J_s = 1 - \frac{D_s}{S_{real}} \quad [7]$$

Where D_s is the sum of the disparity map and S_{real} is the sum of the pixels classified as shadow in the real image. J_s expresses the fraction of pixels in shadows correctly reproduced in the synthetic model.

3. **Contrast index**. A second index is then identified. For both images, the real and the synthetic, an illumination ratio RI is identified as:

$$R_I = \frac{I_L}{I_s} \quad [8]$$

Where I_L is the mean intensity of the pixel classified as in light, and I_S is the mean intensity of the pixel classified as in shadow. Then, the contrast index J_c is defined as:

$$J_c = \frac{R_{Ireal}}{R_{Irend}} \quad [9]$$

4. **Features quality index**. Typical navigation algorithms rely on feature extraction steps, thus a comparison among real and synthetic images is considered a good indication of the similarity of behaviour among the two. The feature quality index (FQI) indicates the similarity of features extracted in two corresponding frames (a real and a synthetic one) and it is defined as:

$$FQI = 1 - \frac{\mu(H_d)}{H_{d,max}} \quad [10]$$

where H_d is the Hamming distance between two corresponding features descriptors and $H_{d,max}$ are the maximum possible hamming distance. The mean value $\mu(H_d)$ is computed on 10 corresponding ORB features [7].

The higher the indexes, the best the image is represented. Requirements to satisfy the validation are based on the scalar shadow index J_s and on the contrast index J_c. In particular, it is required $J_c > 0.90$, $J_s > 0.75$ and $FQI > 0.80$.

5. Results of obtained images

In this section, the images validation results are presented, starting from the moon landing scenario and then examining the debris inspection case.

5.1 *Moon scenario - dense reconstruction results*

In Fig. 5a an image of the Moon diorama taken with the FLIR Chameleon-3 camera is shown; in Fig. 5b it is shown the corresponding image in generated in Pangu [6] from the reconstructed diorama point cloud. The illumination data are recorded exploiting multiple meridians measurements. Results

show that the validation tool is capable to correctly reproduce the pose and the illumination conditions.

In Fig. 6 the disparity between shadow areas is shown. The corresponding index of merit is $J_s = 1 - D_s/S_{real} = 0.82$. As it can be seen, there are still some shadow areas not matched and the requirement is not yet satisfied. The error causes are multiple: the uncertainty in the pose, errors in the determination of the camera intrinsic parameters, the irradiance settings on the point cloud. The black peaks in the synthetic images are mainly due to the presence of holes in the dense point cloud of the facility. A recalibration of the Moon diorama facility has been performed, which solved the problems yielding a successful validation On the other hand, the contrast index requirement is met, being $J_c = 0.80$, showing a good capability of brightness representation.

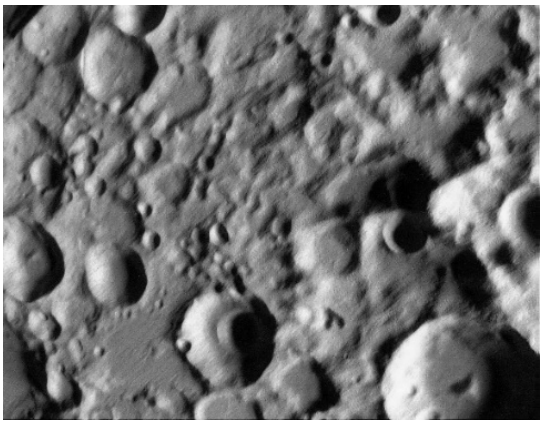

(a) Real laboratory image.

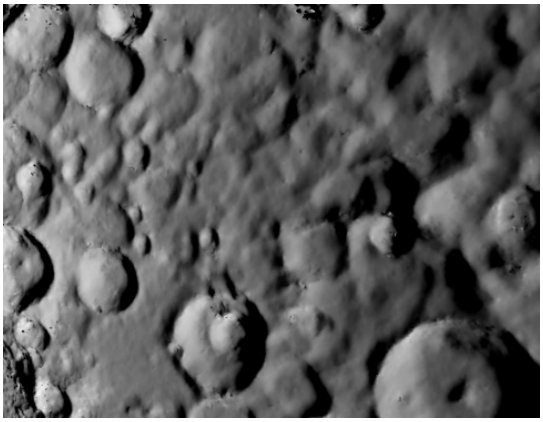

(b) Rendered image.

Fig. 5: Example of laboratory image and Pangu image. Example of real image (left). Example of synthetic image (right). The example refers to the pre-recalibration activities.

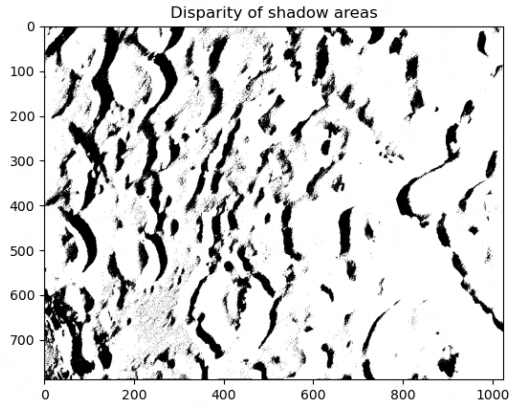

Fig. 6: Disparity map of shadow areas.

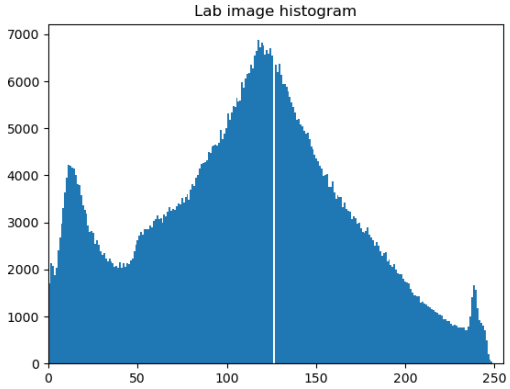

(a) Real laboratory image.

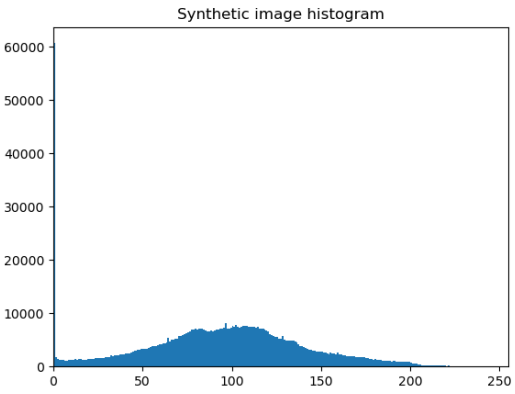

(b) Rendered image.

Fig. 7: Images histograms. Lab image histogram (left). Lab image histogram (right).

As a further insight on the two images, their histograms are shown in Fig. 7. It can be observed that the histogram peak is similar for the two and that in the synthetic image there is the presence of completely black pixels, as expected.

The histograms values are comparable, in particular the central peak. Nevertheless, in the synthetic images a black peak is found, which scales the plots differently. The white peak present in the lab images was due to reflections in the lab, which are aimed to be further minimized. As mentioned, the black peak found in the synthetic image is due to the presence of holes in some region of the diorama mesh used to generate PANGU world.

5.2 *Moon scenario - ground truth results*

The validation campaign aimed at using the robotic facility to acquire real images, to check adequateness of synthetically generated images. The validation images cover different region of the diorama and are taken with different set-up of the facility illumination. The results of the validation campaign (restricted to 10 images so far) are summarized in Table 5. An example of validated images and corresponding histograms, together with the resulting disparity map is shown in Fig. 8, Fig. 10, Fig. 9.

Table 5: Summary of validated images and corresponding indices - Moon scenario.

Frame	$\mathbf{J_s > 0.9}$	$\mathbf{J_c > 0.75}$	**Sun [Az, El]**
0	0.92	0.88	[262°, 56°]
1	0.96	0.79	[84°, 60°]
2	0.91	0.82	[84°, 60°]
3	0.91	0.78	[84°, 60°]
4	0.96	0.78	[84°, 60°]
5	0.92	0.82	[86°, 35°]
6	0.91	1.00	[262°, 41°]
7	0.92	0.97	[86°, 26°]
8	0.91	0.80	[86°, 26°]
9	0.91	0.91	[86°, 26°]
10	0.95	0.91	[86°, 26°]

5.3 *Debris scenario results*

In this section the images obtained for the debris scenario are analysed.

Detailed results are here shown for a sample pose and illumination. The laboratory image and the render are compared with the extracted ORB features in Fig. 11. It can be seen that the pose is correctly retrieved, even if the rigidity of the mock-up's solar panel has to be improved to match the ideal positioning visible from the synthetic image. The extracted features are very close both in number and location;

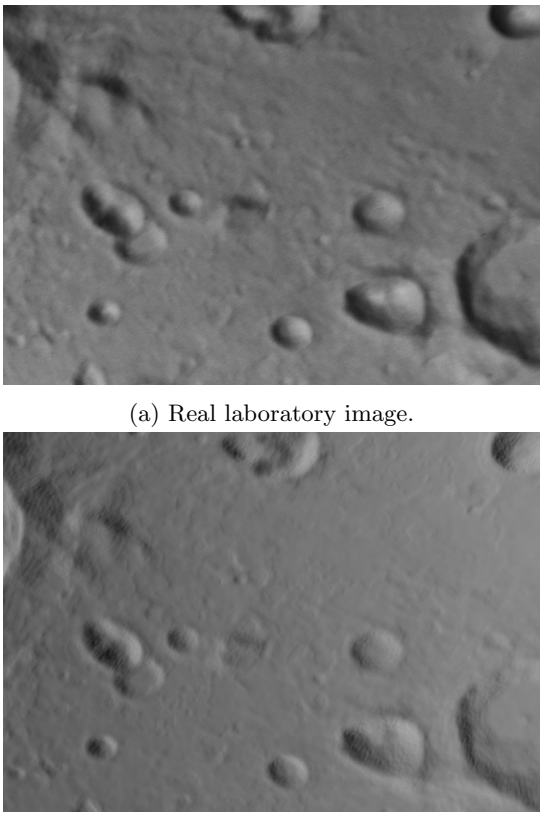

(a) Real laboratory image.

(b) Rendered image.

Fig. 8: Example of laboratory image and Pangu image. Example of real image (left). Example of synthetic image (right).

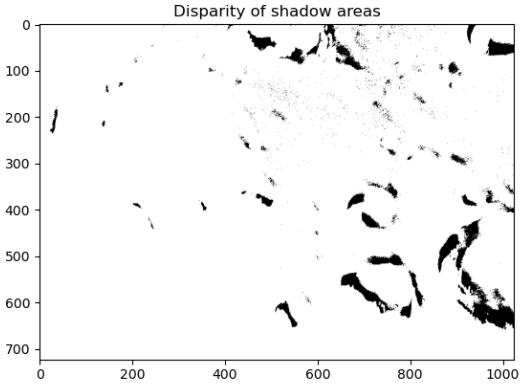

Fig. 9: Disparity map of shadow areas.

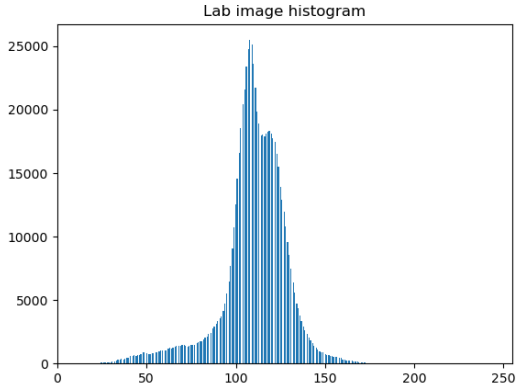

(a) Real laboratory image.

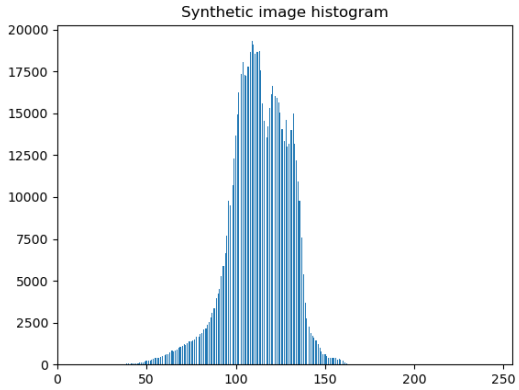

(b) Rendered image.

Fig. 10: Images histograms. Lab image histogram (left). Lab image histogram (right).

the features quality index is $FQI = 0.82$. Please note that in Fig. 11 the marker in the laboratory image has not been cropped, but that the FQI is computed based on corresponding features only. An high FQI indicates that the ORB descriptors are similar in the two images and thus that the illumination and mock-up materials are realistically reproduced.

For the same image couple, the histograms are reported in Fig. 12. The two histograms are not exactly matching, but they are showing a similar trend. The major difference is present for low intensity pixels, and in particular it can be attributed to the diffuse light inevitably present in the facility. The shadow index is $J_s = 0.98$, indicating a shadow distribution very close to the one obtained with the rendered ground truth.

The validation metrics evaluated for a subset of

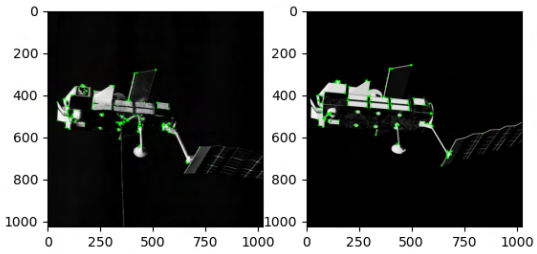

Fig. 11: Example of features extraction comparison.

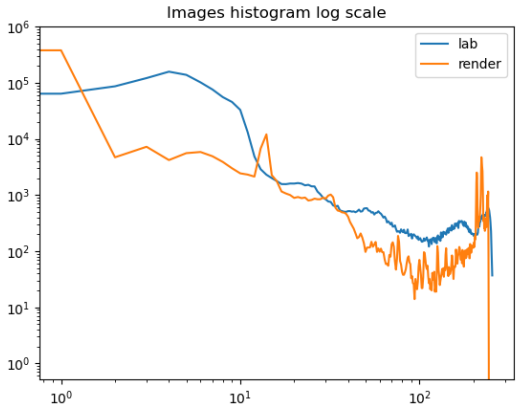

Fig. 12: Example of features histograms comparison.

Table 6: Summary of validated images and corresponding indices - Debris scenario.

Frame	$\mathbf{J_s > 0.9}$	**FQI > 0.8**	**Sun [Az, El]**
0	0.97	0.82	[318°, -28°]
1	0.95	0.83	[120°, -63°]
2	0.91	0.80	[120°, -63°]
3	0.94	0.82	[120°, -63°]
4	0.96	0.80	[120°, -63°]
5	0.94	0.82	[120°, -63°]
6	0.96	0.85	[120°, -63°]
7	0.92	0.82	[120°, -63°]
8	0.94	0.84	[334°, -17°]
9	0.98	0.81	[334°, -17°]
10	0.97	0.82	[334°, -17°]

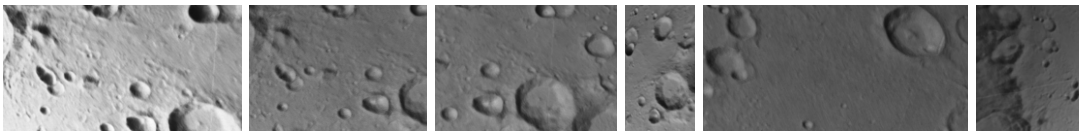

(a) Laboratory images.

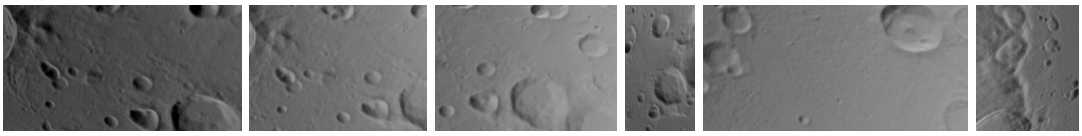

(b) Synthetic images.

Fig. 13: Images from Moon validation set (frames 1 to 6).

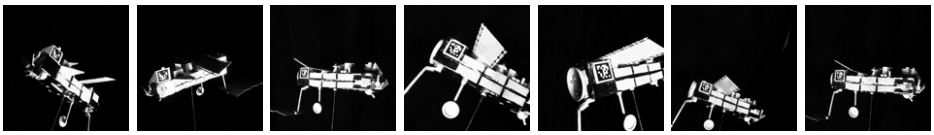

(a) Laboratory images.

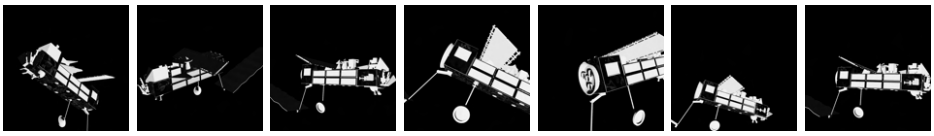

(b) Synthetic images.

Fig. 14: Images from Debris validation set (frames 1 to 7).

10 validated images are shown in Table 6. The images are shown in Fig. 14 and correspond to different poses and illumination conditions. The validation campaign can be considered successfully concluded, and opening the door to tests of traditional and AI-based vision-based navigation algorithms.

6. Conclusions

The paper presented the capabilities of ARGOS experimental facility for on-ground testing of image-based relative navigation technologies. The facility, at PoliMi-DAER premises, is setup and under constant development. The procedures for the facility calibration have been consolidated, including camera calibration, moon diorama dense reconstruction and marker-based pose estimation. Various set-ups are available for on ground testing & validation of relative navigation algorithms. In this paper the setups for a landing scenario and debris fly-around have been examined, successfully validating the obtained images with histograms comparison and with shadows, contrast and features-extraction indices. Future work will include the testing of traditional and AI image-based navigation algorithms in the moon landing and debris fly-around scenario, including PIL tests.

References

[1] OpenCV library. `https://opencv.org/`. Last accessed: September 2021.

[2] Friedrich Fraundorfer and Davide Scaramuzza. Visual odometry: Part ii: Matching, robustness, optimization, and applications. *IEEE Robotics & Automation Magazine*, 19(2):78–90, 2012.

[3] Anders Heyden and Marc Pollefeys. Multiple view geometry. *Emerging topics in computer vision*, 3:45–108, 2005.

[4] Mate Kisantal, Sumant Sharma, Tae Ha Park, Dario Izzo, Marcus Märtens, and Simone D'Amico. Satellite pose estimation challenge: Dataset, competition design, and results. *IEEE Transactions on Aerospace and Electronic Systems*, 56(5):4083–4098, 2020.

[5] Paolo Lunghi, Marco Ciarambino, Marco Marcon, and Michéle Lavagna. A new experimental facility

for testing of vision-based gnc algorithms for planetary landing. In *10th International ESA Conference on Guidance, Navigation & Control Systems (GNC 2017)*, 2017.

[6] Iain Martin, Martin Dunstan, and Manuel Sanchez Gestido. Planetary surface image generation for testing future space missions with pangu. In *2nd RPI Space Imaging Workshop*. Sensing, Estimation, and Automation Laboratory, 2019.

[7] Ethan Rublee, Vincent Rabaud, Kurt Konolige, and Gary Bradski. Orb: An efficient alternative to sift or surf. In *2011 International conference on computer vision*, pages 2564–2571. Ieee, 2011.

[8] Stefano Silvestrini, Paolo Lunghi, Margherita Piccinin, Giovanni Zanotti, and Michèle Lavagna. Artificial intelligence techniques in autonomous vision-based navigation system for lunar landing. In *71st International Astronautical Congress (IAC 2020)*, pages 1–11, 2020.

[9] Stefano Silvestrini, Paolo Lunghi, Margherita Piccinin, Giovanni Zanotti, and Michèle Lavagna. Experimental validation of synthetic training set for deep learning vision-based navigation systems for lunar landing. In *71st International Astronautical Congress (IAC 2020)*, pages 1–10, 2020.